

Brownian search for targets hidden in cusp-like pockets: Progress and Applications

C. Guerrier¹ and D. Holcman^{1 a}

Applied Mathematics and Computational Biology, Ecole Normale Supérieure, 46 rue d'Ulm 75005 Paris, France.

Abstract. We report here recent progress in computing the search time for a stochastic particle to find a small target hidden in cusp-like pockets. The target is a small segment in dimension two, a small hole or a narrow ribbon in dimension three, placed at the end of a cusp. The asymptotic analysis of the diffusion equation reveals the role of the local geometry, and a mathematical difficulty comes from the boundary layer near the target. The methods are conformal mapping and matching asymptotic. We present applications in cell biology where cellular activation occurs when a diffusing particle finds a hidden site. This is the case during vesicular fusion initiated after a protein located between the vesicular and cell membranes binds to several diffusing calcium ions. Another example is a drug activation site located inside a deep molecular pocket. The analytical formulas clarify the role of small parameters.

1 Introduction

Finding a small hidden target by a protein, an ion or a molecule is ubiquitous in molecular and cellular biology, and it represents a key limiting step for activation of a cellular process. For example, proteins need to find active sites hidden in the interior of a larger molecular complex. This is the case for the hemoglobin or the penicillin-binding proteins, and many others where active sites are hidden inside in the complex organization of α and β -sheet structures. For the hemoglobin, a ligand, such as β -lactam antibiotic, has to bind to a small site hidden inside the molecule and indeed, ligand recognition requires that strands should be antiparallel in the active site area [1]. Another example where finding a small target is relevant in cell biology is the diffusion of molecules, RNAs or proteins between the mother and the daughter cell during cell division [2]. The diffusion time is controlled by the arrival of Brownian particles to the cylindrical neck connecting the two cells and it determines the amount of molecules that will be exchanged between them. Interestingly, the mean time for a thin rod to turn in a narrow tube or for a protein to rotate in a thin two-dimensional band is also very long and characterizes a strand to become parallel or anti-parallel.

Contrary to freely accessible small targets, the mean time for a Brownian particle to reach a target located at a narrow cusp is much longer. Finding asymptotic expressions for such search times remains challenging numerically and analytically. Numerically, because it requires very long simulations, leading to many inaccuracies, and this is not even sufficient to guess asymptotic formulas. From an analytical point of view, the classical methods developed for the narrow escape problems do not apply [2–4].

We report recent progress about asymptotic computation of the mean time for a Brownian particle diffusing in a bounded domain to find a small hidden target located at a cusp geometry

^a This research is supported by an ERC-starting-Grant.

on the boundary, which otherwise reflects the particle (Fig. 1). This time is referred in the literature as the Dire Strait Time (DST) [5,6] and differs from the classical narrow escape time (NET), which is the time for a diffusing particle to find a small site located on a smooth part of the boundary.

A major difference between the DST and the NET is reflected in the method for computing asymptotically each search time. In both cases, this computation involves solving the Poisson equation with small Dirichlet and large Neumann parts: the NET methods are matched asymptotic [7–9] or Green’s function [3], but these methods fail to compute the DST because the cusp creates a new boundary layer. For the DST, the method mixes asymptotic analysis and conformal mapping. Furthermore, the analysis in dimension three is possible when there are symmetries that allow the analysis to two dimensions. However in both search, because they are rare events, the probability density function of the time spent $\bar{\tau}$ in a compartment prior to escape, in the limit of small target size, is dominated by a single exponential decay

$$p_{\bar{\tau}}(t) \sim \bar{\tau}^{-1} \exp\{-t/\bar{\tau}\}. \quad (1)$$

The exponential rate $\bar{\tau}^{-1}$ is therefore the flux into the absorbing target. This single exponential result allows coarse-graining microscopic model of reaction-diffusion into Markovian jump processes, where the rate is the flux on the absorbing boundary equal to the reciprocal of $\bar{\tau}$. This rate encompasses the entire geometry to a single parameter, and can be used to simplify detailed stochastic simulations of biological pathways by replacing long stochastic trajectories with Poissonian injection rate.

Finally, the local shape of the target does matter for the search time, as revealed both by analytical and numerical methods [10–14]. For example, an elliptic versus circular disc changes the leading order of the search time, and the exit time to two tangent discs versus a single disc of similar surface is different [3]. This report is organized as follows: in section 2, we present several examples motivated by cellular biology in which computing the DST is a key to understand the role of small targets. In section 3, we present a general classification for targets hidden in cusps. We also discuss the case of an absorbing band at the cusp between a plane and a sphere (Fig. 2D).

2 Examples for the search of a hidden target in cellular and molecular biology

2.1 Mother-daughter cell

An intermediate stage during cell division consists of the asymmetric dumbbell shape (Fig. 2A) made between the mother and daughter cells, separated by a long connecting neck that can change over time. During this stage, some of the genetic material is transferred from the mother to the smaller daughter cell compartment. Diffusion through the cusps connecting the neck is the main determinant of the exchange rate and of the selection of fast diffusing particles during this transient regime [15]. Moreover, in the absence of any active mechanism, the back flow induced by diffusion from the daughter to the mother cell can be drastically slowed down, due to an asymmetry in the curvature of the connecting neck between cells. Thus the transition rates between the mother and the daughter can differ by several orders of magnitude as the geometry at the cusp changes. This asymmetrical diffusion effect can explain some of the findings reported experimentally in [15]: as the curvature at the connection between the cells and the neck varies over time, it changes the diffusion fluxes, as indicated by first passage time formulas that we shall describe below (see equation 18 and [2]). In conclusion, small asymmetric diffusion fluxes permit to isolate the mother from the daughter cells prior to reaching steady state. Had steady state diffusion been reached before the two cells separated, the probability density function of diffusing particles would be uniform in the domain, and the amount of particles in both cells would be proportional to their volumes.

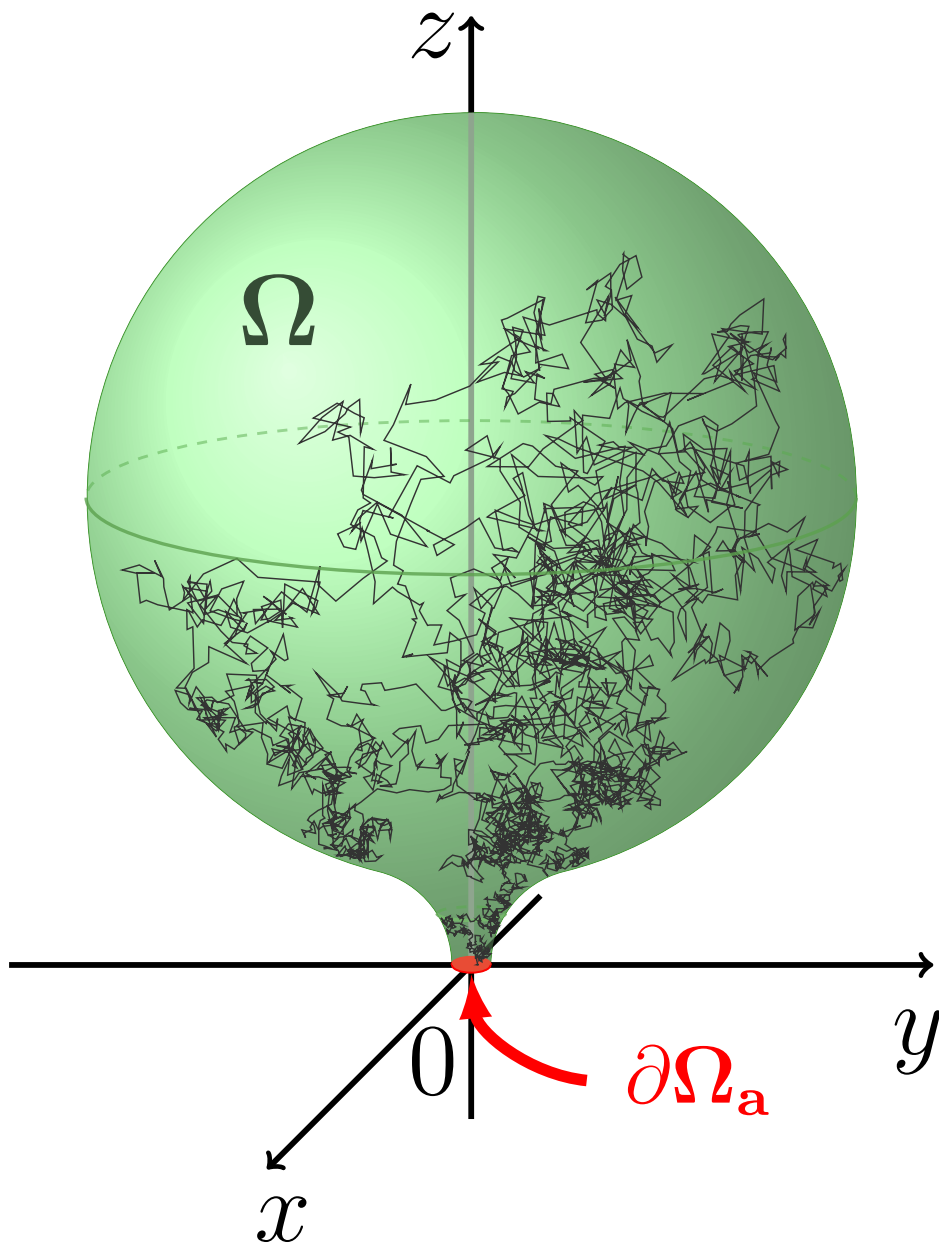


Fig. 1. Schematic description of the exit search through a cusp.

2.2 Finding a binding site in a protein: the example of hemoglobin

Active sites of complex molecules, such as hemoglobin, can be hidden inside a complex molecular organization (Fig. 2B). To become activated, a ligand has to bind to a small site hidden inside the molecule and indeed, ligand recognition requires that strands be well positioned in the active site area. This phenomenon was observed for large antibiotic molecules such as the penicillin-binding proteins [1]: the catalytic funnel reveals an elongated binding cleft, where the active site is hidden. When the site can switch between an active and inactive state, the effective rate constant changes drastically [2].

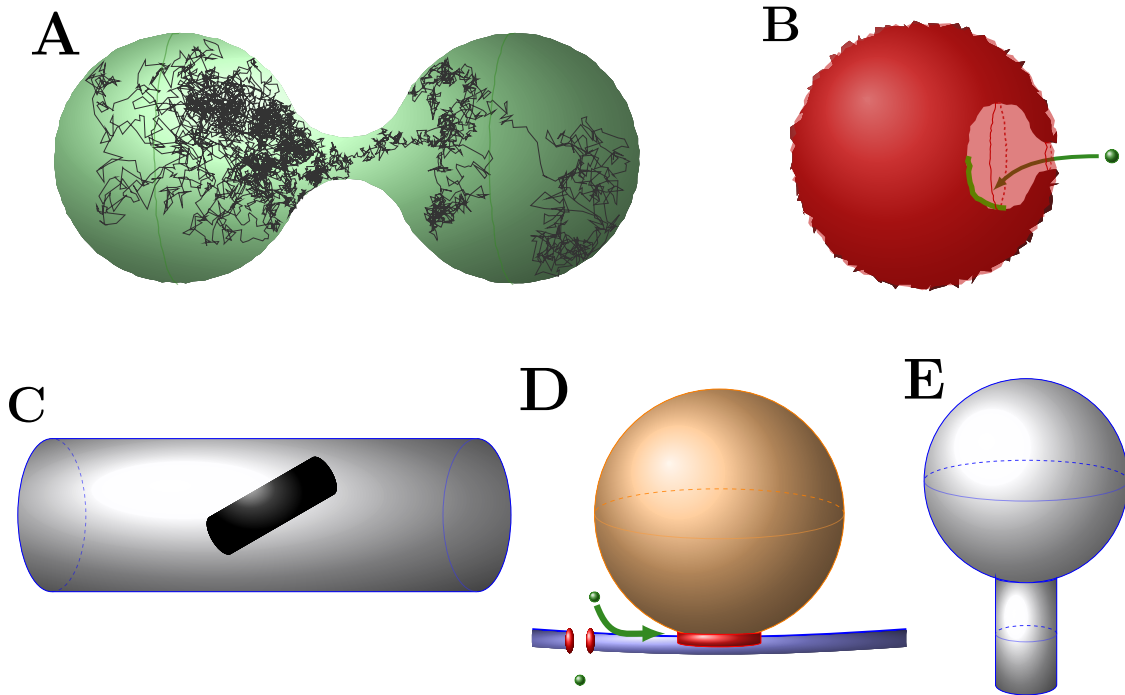


Fig. 2. Schematic cusp targets in cell biology characterized by the DST. **A:** Model of diffusion between the mother and daughter cell through a cusp and narrow neck. **B:** Search by a molecule of a binding site, hidden in a cusp geometry. **C:** Rotation of a rod-like molecule in a cylindrical narrow domain. The rotation can only occur in an extreme position, representing a cusp in the phase space. **D:** The binding of several calcium ions (green) to a group of molecules located at the cusp (red) between the docked vesicle (orange) and the neuronal membrane (blue), induces vesicular release at the pre-synaptic terminal. **E:** The particular shape of the post-synaptic dendritic spine can be represented by a bulky head connected to a thin neck. Ions entering at the PSD on the top of the head escape the spine at the bottom of the neck.

2.3 Rotation of a needle in a confined band

A Brownian needle in a strip can model a stiff DNA fragment moving in a very confined chromatin structure. For example, under severe stress, the DNA of the bacterium *Deinococcus radiodurans*, the most radioresistant organism, undergoes a phase transition in reorganizing its genome into tightly packed toroids, which may facilitate DNA repair [16]. Three-dimensional analyses [17] reveal a complex network of double membranes that engulf the condensed DNA, suggesting that two-dimensional domains lying between parallel walls may play a significant role in DNA repair. The role of the distance between the parallel walls can be evaluated in the computation of the mean time for a needle to rotate in such environment (see equation 15). A similar example is a planar strip or a three dimensional cylinder: when a needle is only slightly shorter than the strip width, its turning around becomes a rare event, because there is not much room in the configuration space for the vertical position (Fig. 2C). Thus the computation of the mean time to turn around becomes a Dire Strait problem [3], which does not fall under the previously studied NET in planar geometry [3, 7–9, 13, 18–20].

2.4 Cusp activation between a vesicle and the pre-synaptic membrane of a neuron

Another illustration of cusp geometry that controls cellular processes from the molecular level is calcium diffusion near a vesicle located in the pre-synaptic terminal. Indeed calcium diffusion determines the probability of vesicular release (Fig. 2D), which should depend on the distance

between the initial calcium entrance at channels and the docked vesicle position. Specifically, after ions enter the pre-synaptic terminal through calcium channels, they have to bind to specific proteins located at the junction between the vesicle and the membrane that we shall modeled here as a ribbon (red in Fig. 2D). Interestingly, the probability of vesicular release can vary over 6 order of magnitude for the same synapse, a phenomenon that is still not clearly understood [21,22]. The particular cusp geometry formed by the vesicle and the pre-synaptic membrane might be a key to resolve this drastic probability modulation [23].

3 Classification of the NET and DST in dimension two and three

3.1 Stochastic equation

A Brownian particle escapes through a narrow cusp located on the surface of a bounded domain Ω (see the example in Fig. 1). The motion is described by the stochastic equation

$$\dot{\mathbf{X}} = b(\mathbf{X}) + \sqrt{2\mathcal{D}}\dot{\mathbf{w}} \quad (2)$$

where b is the drift, \mathcal{D} is the diffusion coefficient and $\dot{\mathbf{w}}$ is white noise. We will consider $b = 0$ (for non-zero drift, new Non-Poissonian escape rates have recently been discussed in [24]). The DST $\bar{\tau}(\mathbf{x})$ for a particle starting at position \mathbf{x} is the solution of [25]

$$\begin{aligned} \mathcal{D}\Delta\bar{\tau}(\mathbf{x}) &= -1 \text{ for } \mathbf{x} \in \Omega \\ \frac{\partial\bar{\tau}}{\partial n}(\mathbf{x}) &= 0 \text{ for } \mathbf{x} \in \partial\Omega \setminus \partial\Omega_a \\ \bar{\tau}(\mathbf{x}) &= 0 \text{ for } \mathbf{x} \in \partial\Omega_a, \end{aligned} \quad (3)$$

where $\partial\Omega$ (resp. $\partial\Omega_a$) is the boundary (resp. the absorbing part of the boundary).

3.2 Dire strait formula in dimension 2

We now summarize classical results about the NET and DST from a domain Ω in the plane, for a small absorbing arc $\partial\Omega_a$ of length a of the boundary $\partial\Omega$. The ratio between the arclength of the absorbing boundary and the arclength of the entire boundary is a small parameter

$$\varepsilon = \frac{|\partial\Omega_a|}{|\partial\Omega|} = \frac{a}{|\partial\Omega|} \ll 1. \quad (4)$$

When $\partial\Omega_a$ is a sub-arc of a smooth boundary, the first order in ε of the NET from any point \mathbf{x} in Ω to $\partial\Omega_a$, denoted by $\bar{\tau}_{\mathbf{x} \rightarrow \partial\Omega_a}$, is independent of \mathbf{x} outside a small vicinity of $\partial\Omega_a$ (called a boundary layer), and we have

$$\bar{\tau}_{\mathbf{x} \rightarrow \partial\Omega_a} = \frac{|\Omega|}{\pi\mathcal{D}} \ln \frac{1}{\varepsilon} + O(1), \quad (5)$$

where $O(1)$ depends on the initial distribution of \mathbf{x} [8,20]. In particular, if Ω is a disc of radius R , then for \mathbf{x} at the center of the disc,

$$\bar{\tau}_{\mathbf{x} \rightarrow \partial\Omega_a} = \frac{R^2}{\mathcal{D}} \left[\ln \frac{\pi R}{a} + 2 \ln 2 + \frac{1}{4} + O(\varepsilon) \right], \quad (6)$$

and averaging with respect to a uniform distribution of \mathbf{x} in the disc [3]

$$\bar{\tau} = \frac{R^2}{\mathcal{D}} \left[\ln \frac{\pi R}{a} + 2 \ln 2 + \frac{1}{8} + O(\varepsilon) \right]. \quad (7)$$

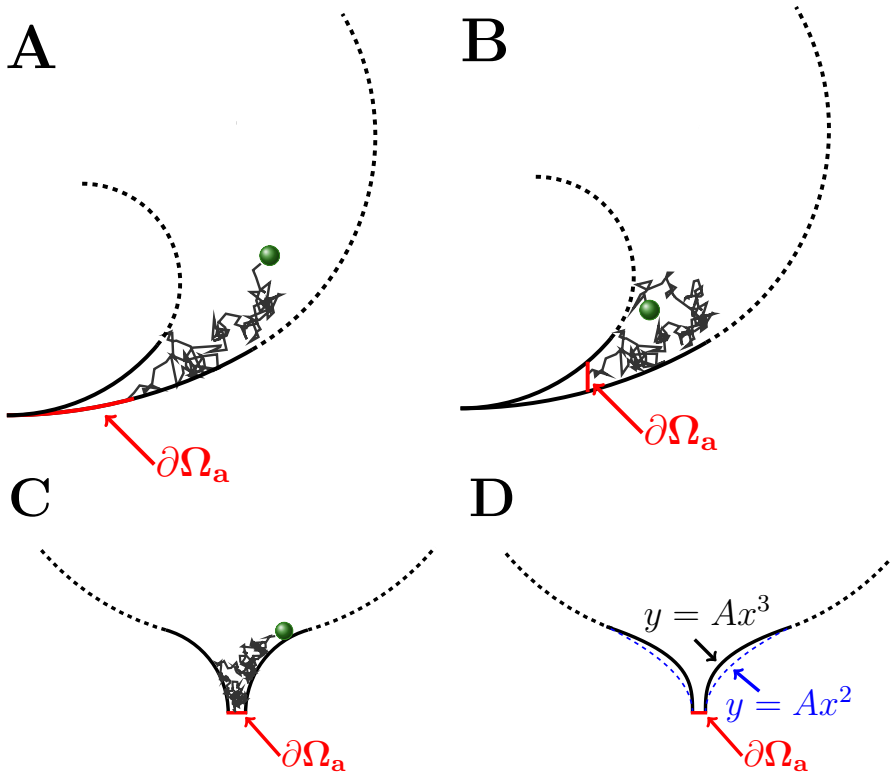


Fig. 3. Classification of cusp targets. Target tangent **A**, perpendicular **B** and at the end **C** of a cusp. Changing the order of approximation of the cusp **D**.

Formula 5 indicates that the flux through a hole in a smooth wall on a flat membrane surface (e.g., a corral) is regulated by the following parameters: the area $|\Omega|$, the diffusion coefficient \mathcal{D} , and the aspect ratio ε (equation 4). This asymptotic formula can be used to estimate the residence time of a receptor inside the post-synaptic density, a main factor governing short-term synaptic plasticity [2].

For a Brownian motion on a sphere of radius R , described in the spherical coordinates (θ, ϕ) where $(x, y, z) = (R \sin \theta \cos \phi, R \sin \theta \sin \phi, R \cos \theta)$, the NET to an absorbing circle centered at the north-south axis ($\theta = 0$) near the south pole with a radius $a = R \sin \delta/2 \ll 1$, is given by

$$\bar{\tau}_{\mathbf{x} \rightarrow \partial\Omega_a} = \frac{2R^2}{\mathcal{D}} \ln \frac{\sin \frac{\theta}{2}}{\sin \frac{\delta}{2}}, \quad (8)$$

where $\delta \leq \theta \leq \pi$ [2]. Formula 8 can be used to estimate the rate of accumulation at one pole of proteins moving on the membrane surface during embryo development [26].

When the absorbing window in a plane is no longer on a smooth surface, but located at a corner of angle α , then ([3])

$$\bar{\tau}_{\mathbf{x} \rightarrow \partial\Omega_a} = \frac{|\Omega|}{\mathcal{D}\alpha} \left[\ln \frac{1}{\varepsilon} + O(1) \right]. \quad (9)$$

Formula 9 indicates that control of flux is regulated also by the access to the absorbing window afforded by the the angle of the corner leading to the window.

If the absorbing window is located at a cusp, then $\bar{\tau}_{\mathbf{x} \rightarrow \partial\Omega_a}$ grows algebraically, rather than logarithmically. In the domain bounded by two tangent circles (Fig. 3A), the lifetime is

$$\bar{\tau}_{\mathbf{x} \rightarrow \partial\Omega_a} = \frac{|\Omega|}{(d^{-1} - 1)\mathcal{D}} \left(\frac{1}{\varepsilon} + O(1) \right), \quad (10)$$

where $d < 1$ is the ratio of the radii [3]. Formula 10 indicates that a drastic reduction of flux can be achieved by putting an obstacle that limits the access to the absorbing window by forming a cusp-like passage. In addition, when $\partial\Omega_a$ is located at the end of a narrow neck with radius of curvature R_c (Fig. 3C-D), the DST is given in [2,27] as

$$\bar{\tau}_{\mathbf{x} \rightarrow \partial\Omega_a} = \frac{\pi|\Omega|}{2\mathcal{D}\sqrt{a/R_c}} (1 + o(1)) \quad \text{for } a \ll |\partial\Omega|. \quad (11)$$

Formula 11 can be used to estimate the effective diffusion coefficient from a model of disk obstacles located on a lattice [2,27].

The DST can also be computed on a surface of revolution generated by rotating a curve around an axis of symmetry. For example, the rotation of the curve in Fig. 3C around its axis of symmetry leads to a three dimensional domain similar to Ω in Fig. 1. We use the representation of the generating curve

$$y = r(x), \quad 0 < x < \Lambda$$

where the x -axis is horizontal with $x = \Lambda$ at the absorbing end \mathbf{AB} . We assume that the parts of the curve that generate the funnel have the form

$$\begin{aligned} r(x) &= O(\sqrt{|x|}) \quad \text{near } x = 0 \\ r(x) &= a + \frac{(x - \Lambda)^{1+\nu}}{\nu(1+\nu)\ell^\nu} (1 + o(1)) \quad \text{for } \nu > 0 \text{ near } x = \Lambda, \end{aligned} \quad (12)$$

where $a = \frac{1}{2}\overline{\mathbf{AB}}$ is the radius of the gap, and the constant ℓ has dimension of length. For $\nu = 1$ the parameter ℓ is the radius of curvature R_c at $x = \Lambda$. The DST from the head to the absorbing end \mathbf{AB} is given by the following algebraic decay [6]

$$\bar{\tau}_{\mathbf{x} \rightarrow \partial\Omega_a} \sim \frac{\mathcal{S}(\Lambda)}{2\mathcal{D}} \frac{\left(\frac{\ell}{(1+\nu)a}\right)^{\nu/(1+\nu)} \nu^{1/(1+\nu)}}{\sin \frac{\nu\pi}{1+\nu}}, \quad (13)$$

where \mathcal{S} is the entire unscaled area of the surface. In particular, for $\nu = 1$ the DST 13 reduces to

$$\bar{\tau}_{\mathbf{x} \rightarrow \partial\Omega_a} \sim \frac{\mathcal{S}}{4\mathcal{D}\sqrt{a/2\ell}}. \quad (14)$$

The case $\nu = 0$ corresponds to a conical funnel with an absorbing circle of small radius a (see [6]). For a sphere, equation 14 reduces to 8. Formulas 11–14 indicate that an efficient control of the flux can be achieved by putting the absorbing window at the end of a narrow symmetric or asymmetric funnel. This type of funnel can be formed by crowding obstacles on the membrane surface [27], which results in an effective coarse-grained diffusion coefficient on the surface, different from the microscopic diffusion coefficient. Finding the NET in the flat plane when the cusp locally behaves like $y(x) = Ax^\alpha + o(x^{\alpha+1})$ with $\alpha > 2$ remains an open problem (see Fig. 3C-D).

The turning around of a needle of length l confined to a planar strip which is only slightly wider (length l_0) than the length of the neck can be reduced to a two-dimensional DST problem through a funnel (see Fig. 2C and subsection 2.3 for a specific description of biological motivations). The DST for the needle to turn 180° is given by [3]

$$\bar{\tau} = \frac{\pi(\pi/2 - 1)}{D_r l_0 \sqrt{\varepsilon}} \sqrt{\frac{D_X}{D_r}} (1 + O(\sqrt{\varepsilon})). \quad (15)$$

where $\varepsilon = \frac{l_0 - l}{l_0} \ll 1$, D_X is the longitudinal diffusion constant along the axis of the needle and D_r the rotational constant (see [28–30] for a specific description of the Brownian motion

of anisotropic objects such as a needle in two dimensions). Formula 15 shows that when the free space between two planes decreases, the effective diffusion constant, proportional to the reciprocal of $\bar{\tau}$, experiences a second order phase transition characterized by a discontinuity of the derivative of the effective diffusion constant for the rotation. When the length l reaches and exceeds the critical value l_0 , the diffusion constant vanishes. This result explains the crucial role of the chromatin organization in maintaining the genome integrity after radiation.

Another illustration of the DST can be found in the problem of diffusion escape from a dendritic spine membrane, or from cell during its division. Dendritic spines can be modeled as domains with a bulky head connected to an essentially one-dimensional strip (or cylinder) of small radius a and length L (Fig. 2E). The connection of the head (Ω_1) to the neck (Ω_2) can form either an angle or a smooth funnel. The boundary of the domain reflects Brownian trajectories and only the end of the cylinder $\partial\Omega_a$ absorbs them. In the three-dimensional case the Dirichlet boundary $\partial\Omega_a$ is a small absorbing disc at the end of the cylinder. The domain Ω_1 is connected to the cylinder at an interface $\partial\Omega_i$, which in this case is a circle. It was shown in [6] that the DST from $\mathbf{x} \in \Omega_1$ to $\partial\Omega_a$ is given by

$$\bar{\tau}_{\mathbf{x} \rightarrow \partial\Omega_a} = \bar{\tau}_{\mathbf{x} \rightarrow \partial\Omega_i} + \frac{L^2}{2\mathcal{D}} + \frac{|\Omega_1|L}{|\partial\Omega_a|\mathcal{D}}. \quad (16)$$

Formula 16 shows the role of the narrow neck in the diffusion flux regulation.

3.3 Dire strait formula in dimension 3

We recall now some known mean time asymptotic expressions for the NET in a three-dimensional domain Ω when the target is a circular absorbing window $\partial\Omega_a$ of radius a centered at $\mathbf{0}$ on the boundary $\partial\Omega$. It is given by [3]

$$\bar{\tau}_{\mathbf{x} \rightarrow \partial\Omega_a} = \frac{|\Omega|}{4a\mathcal{D}} \left[1 - \frac{L(\mathbf{0}) + N(\mathbf{0})}{2\pi} a \ln a + O(a) \right], \quad (17)$$

where $L(\mathbf{0})$ and $N(\mathbf{0})$ are the principal curvatures of the surface boundary at the center of the absorbing boundary $\partial\Omega_a$. The third order asymptotic expansion can be found on a sphere [31]. This formula is contrast with the DST asymptotics obtained for a target hidden in a three dimensional cusp. When the target is a small absorbing window $\partial\Omega_a$ of radius a located at the end of a funnel (Fig. 1), the asymptotics is

$$\bar{\tau}_{\mathbf{x} \rightarrow \partial\Omega_a} = \left(\frac{R}{a} \right)^{3/2} \frac{|\Omega|}{R\mathcal{D}} (1 + o(1)) \text{ for } a \ll R, \quad (18)$$

where the R is the radius of curvature of the rotated curve at the end of the funnel [6]. This formula corrects by a factor 1/2 the previous one reported in [2,6]. The dependency in the radius of curvature at the cusp explains how geometry controls the diffusion flux from the mother to the daughter cell, as explained above in subsection 2.1. This asymptotics can also be used to estimate the search time for a hidden target inside a molecule (see subsection 2.2)

Finally, the last asymptotic formula we shall present has application to estimate the probability of vesicular release at synapse for a model of calcium diffusion. The cusp-like geometry between a sphere and a surface (subsection 2.4 and [23] and Fig. 2D). The two-dimensional projection near the cusp is represented in Fig. 3B. The DST a three-dimensional cusp, located at the end of a funnel when the absorbing cross section is perpendicular to the cusp is given by

$$\bar{\tau}_{\mathbf{x} \rightarrow \partial\Omega_a} = \frac{|\Omega|}{4\pi\mathcal{D}a} + O(1). \quad (19)$$

The absorbing boundary forms a small ribbon of height a with surface $S_{rib} = \sqrt{2 \frac{R_1 R_2}{|R_2 - R_1|}} a^{3/2}$ where R_1 and R_2 are the radii of curvature at the cusp. This result is presented below in subsection 3.5.

3.4 Derivation of the DST for a three-dimensional cusp located at the end of a funnel

We now present the main steps to compute the DST (formula 18) for a target located at the end of a cusp (Fig. 1). We use a conformal mapping to map the domain Ω that contains a small absorbing window $\partial\Omega_a$ of diameter a located at the end of the funnel, which is connected smoothly to a three dimensional ball. The radius of curvature at the funnel is R and the diffusion coefficient is \mathcal{D} . The symmetric cusp can be parameterized in cylindrical coordinates (ρ, z) (ρ is the distance to the $0z$ axis) by

$$\rho(z) = \frac{1}{R}z^2 + \frac{a}{2}, \quad (20)$$

for z small. In dimensionless variables $\mathbf{x} = R\mathbf{x}'$, $\bar{\tau}(\mathbf{x}) = u(\mathbf{x}')$, the domain Ω is mapped on Ω_{dless} , $\partial\Omega_a$ into $\partial\Omega_{\text{dless},a}$ and $|\Omega| = R^3|\Omega_{\text{dless}}|$, $a = R\epsilon$, $\mathcal{D} = R^2D$. The DST equation 4 becomes:

$$\begin{aligned} D\Delta u(\mathbf{x}') &= -1 \text{ for } \mathbf{x}' \in \Omega_{\text{dless}} \\ \frac{\partial u}{\partial n}(\mathbf{x}') &= 0 \text{ for } \mathbf{x}' \in \partial\Omega_{\text{dless}} \setminus \partial\Omega_{\text{dless},a} \\ u(\mathbf{x}') &= 0 \text{ for } \mathbf{x}' \in \partial\Omega_{\text{dless},a}, \end{aligned} \quad (21)$$

In cylindrical coordinates (ρ, ψ, z) , due to symmetry, the equation reduces to

$$\begin{aligned} \frac{\partial^2 u}{\partial \rho^2} + \frac{1}{\rho} \frac{\partial u}{\partial \rho} + \frac{\partial^2 u}{\partial z^2} &= -\frac{1}{D} \text{ for } (\rho, z) \in \Omega_{\text{dless}} \\ \frac{\partial u}{\partial n}(\rho, z) &= 0 \text{ for } (\rho, z) \in \partial\Omega_{\text{dless}} \setminus \partial\Omega_{\text{dless},a} \\ u(\rho, z) &= 0 \text{ for } (\rho, z) \in \partial\Omega_{\text{dless},a}. \end{aligned} \quad (22)$$

Using Mobius mapping

$$f(\xi) = \frac{\xi - \alpha_\epsilon}{\xi + \alpha_\epsilon}, \quad (23)$$

where $\xi = \rho + iz$, we map the two-dimensional domain $\Omega_{2D} = \Omega_{\text{dless}} \cap \{\psi = 0\}$ into Γ (Fig. 4), where $\alpha_\epsilon = \sqrt{\epsilon(1 + \epsilon/4)}$. The domain Ω_{2D} is thus mapped into two concentric circles, and the absorbing part of the boundary $\partial\Omega_{2D,a}$ into the segment $\partial\Gamma_a = [-1; -1 + \sqrt{\epsilon}]$ of length $\sqrt{\epsilon}$. The cusp is mapped on a narrow hot-dog shaped domain, and the other part of the domain is mapped on a small region, located at angle $O(\sqrt{\epsilon})$ (Fig. 4). Equation 22 becomes in polar coordinates $\omega = r e^{i\theta} = f(\xi)$ with $v(r, \theta) = u(f^{-1}(\omega))$,

$$\frac{|1 - \omega|^4}{4\alpha_\epsilon^2} \Delta v + \frac{|1 - \omega|^2}{\alpha_\epsilon(1 - |\omega|^2)} \left[\frac{\partial v}{\partial r} \frac{\partial r}{\partial \rho} + \frac{\partial v}{\partial \theta} \frac{\partial \theta}{\partial \rho} \right] = -\frac{1}{D} \text{ for } (r, \theta) \in \Gamma. \quad (24)$$

To solve equation 24 in Γ , we proceed as in [27] and neglect the variation in the r -variable, because $r = 1 + O(\sqrt{\epsilon})$ and thus $v(r, \theta) \approx v(\theta)$ with absorbing boundary condition at π ($v(\pi) = 0$) and a boundary reflection is imposed on the upper part ($v'(c\sqrt{\epsilon}) = 0$), where the constant $c = O(1)$. We find

$$v''(\theta) + \frac{\sin(\theta)}{\cos(\theta) - 1} v'(\theta) = -\frac{\alpha_\epsilon^2}{D(\cos(\theta) - 1)^2}. \quad (25)$$

which is solved as [23]

$$v(\theta) = \frac{|\Omega_{\text{dless}}|}{D\pi\epsilon\sqrt{\epsilon}} (\sin(\theta) + \pi - \theta) + \frac{\alpha_\epsilon^2}{15D} \left[2 \ln \left(\frac{1 - \cos(\theta)}{2} \right) - 2(1 + \cos(\theta)) + \frac{3}{\cos(\theta) - 1} - \frac{3}{2} \right] \quad (26)$$

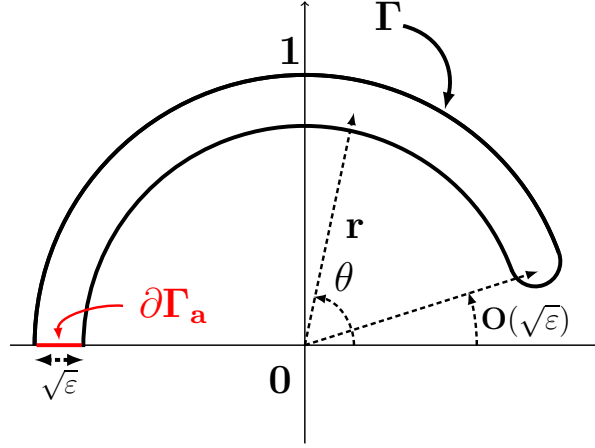


Fig. 4. Mapped Domain. The two-dimensional projection Ω_{2D} of domain Ω_{dless} (dimensionless domain coming from Ω , Fig. 1) is mapped through the Möbius function $f(\xi) = \frac{\xi - \alpha_\epsilon}{\xi + \alpha_\epsilon}$ into Γ .

where $\alpha_\epsilon^2 = O(\epsilon)$. Thus, the mean first passage time $\bar{\tau}_{\mathbf{x} \rightarrow \partial\Omega_a}$ from a point \mathbf{x} inside the domain Ω located outside of the cusp to the absorbing target is obtained by placing the initial point at the angle $\theta = c\sqrt{\epsilon}$ in equation 26. We obtain

$$\bar{\tau}_{\mathbf{x} \rightarrow \partial\Omega_a} = \frac{|\Omega|\sqrt{R}}{\mathcal{D}a\sqrt{a}} + O(1), \quad (27)$$

where R is the curvature at the cusp, \mathcal{D} is the diffusion coefficient and $|\Omega|$ is the total volume of the domain. This formula corrects by a factor 2 the asymptotic expansion for the DST derived in [2, 3, 6].

3.5 Dire strait to a ribbon

To model the probability and the mean time for an ion to find a small target located between a membrane and a vesicle (Fig. 2D and subsections 2.4 and 3.4), we approximate the local geometry by two tangent balls of radii R_1 and R_2 ($R_1 \ll R_2$). We summarize here recent progress on computing the escape time for a Brownian particle to a small ribbon, which consists of a cylinder with small height $a \ll 1$, located between the two spheres (see Fig. 2D and Fig. 3B for two-dimensional projection). In that context, the classical narrow escape results presented in the above sections do not apply. Using the symmetry of the domain, the analysis can be reduced to two-dimensions. In projection, the absorbing ribbon consists of a segment ($\partial\Omega_a$) joining the two discs (see Fig. 3B). Eq. 4 in cylindrical coordinates (r, z) becomes

$$\begin{aligned} \frac{\partial^2 \bar{\tau}}{\partial r^2}(r, z) + \frac{1}{r} \frac{\partial \bar{\tau}}{\partial r}(r, z) + \frac{\partial^2 \bar{\tau}}{\partial z^2}(r, z) &= -\frac{1}{\mathcal{D}} \quad \text{for } (r, z) \in \Omega \\ \frac{\partial \bar{\tau}}{\partial n}(r, z) &= 0 \quad \text{for } (r, z) \in \partial\Omega \setminus \partial\Omega_a \\ \bar{\tau}(r, z) &= 0 \quad \text{for } (r, z) \in \partial\Omega_a. \end{aligned} \quad (28)$$

It is possible to obtain an analytical solution using the inversion mapping $\omega = f(\xi) = 1/\xi$ where $\xi = r + iz$ [23],

$$\bar{\tau}(r, z) = \frac{|\Omega|}{4\pi\mathcal{D}a} \left(1 - 2Ra \left(\frac{r}{r^2 + z^2} \right)^2 \right), \quad (29)$$

where $R = \frac{R_1 R_2}{R_2 - R_1}$. The DST is the mean first passage time $\bar{\tau}_{\mathbf{x} \rightarrow \partial \Omega_a}$ estimated for $r = 0$ in equation 29:

$$\bar{\tau}_{\mathbf{x} \rightarrow \partial \Omega_a} = \frac{|\Omega|}{4\pi \mathcal{D}a} + O(1). \quad (30)$$

This result is quite surprising: the leading order term does not depend on the curvature at the cusp and diverges like $\frac{1}{a}$, which is the divergence behavior for a small circular hole. However, the difference is the surface of the ribbon equals to $S_{rib}(a) = \sqrt{2Ra}^{3/2}$.

4 Conclusion

We have summarized here results about the DST, which is the search time by a Brownian particle of a small target hidden in a cusp. These analytical formulas reveal the role of the local geometrical structure at a molecular level, and show the role of small parameters in controlling diffusion fluxes.

The computation of the DST for cusps of arbitrary shapes remains difficult and very few results exist so far. The presented formulas can be extended in some cases when a drift term is added [24], but in most cases it remains open. The drift term can account for both passive hydrodynamics flow or active transport, such as cargos transported by motors along microtubules. It can also represent the statistical transport driven by electro-diffusion forces.

References

1. P. Macheboeuf, A.M. Di Guilmi, V. Job, T. Vernet, O. Dideberg, and A. Dessen. Active site restructuring regulates ligand recognition in class A penicillin-binding proteins. *Proc. Natl. Acad. Sci. U.S.A.*, 102(3), 2005.
2. D. Holcman and Z. Schuss. Control of flux by narrow passages and hidden targets in cellular biology. *Phys Progr. Report*, 76(7), 2013.
3. D. Holcman and Z. Schuss. The narrow escape problem. *SIAM Review*, 56(6), 2014.
4. D. Holcman and Z. Schuss. Time scale of diffusion in molecular and cellular biology. *Journal of Physics A: Mathematical and Theoretical*, 47(17), 2014.
5. D. Holcman and Z. Schuss. Diffusion laws in dendritic spines. *The Journal of Mathematical Neuroscience*, 1(10), 2011.
6. D. Holcman and Z. Schuss. Brownian motion in dire straits. *SIAM. J. on Multiscale Modeling and Simulation*, 2012.
7. M.J. Ward, W.D. Henshaw, and J.B. Keller. Summing logarithmic expansions for singularly perturbed eigenvalue problems. *SIAM J. Appl. Math.*, 53(3), 1993.
8. M.J. Ward and J.B. Keller. Strong localized perturbations of eigenvalue problems. *SIAM J. Appl. Math.*, 53(3), 1993.
9. M.J. Ward and E. Van De Velde. The onset of thermal runaway in partially insulated or cooled reactors. *IMA J. Appl. Math.*, 48(1), 1992.
10. A.M. Berezhkovskii, L. Dagdug, V.A. Lizunov, J. Zimmerberg, and S.M. Bezrukov. Communication: Clusters of absorbing disks on a reflecting wall: competition for diffusing particles. *J. Chem. Phys.*, 136(21), 2012.
11. A.M. Berezhkovskii, L. Dagdug, V.M. Vazquez, V.A. Lizunov, J. Zimmerberg, and S.M. Bezrukov. Trapping of diffusing particles by clusters of absorbing disks on a reflecting wall with disk centers on sites of a square lattice. *J. Chem. Phys.*, 138(6), 2013.
12. O.K. Dudko, A.M. Berezhkovskii, and G.H. Weiss. Rate constant for diffusion-influenced ligand binding to receptors of arbitrary shape on a cell surface. *J. Chem. Phys.*, 121(3), 2004.
13. I.V. Grigoriev, Y.A. Makhnovskii, A.M. Berezhkovskii, and V.Y. Zitserman. Kinetics of escape through a small hole. *J. Chem. Phys.*, 116(22), 2002.
14. D. Holcman and Z. Schuss. Diffusion escape through a cluster of small absorbing window. *J. Phys. A: Math. and Theoretical*, 41, 2008.

15. L.R. Gehlen, S. Nagai, K. Shimada, P. Meister, A. Taddei, and S.M. Gasser. Nuclear geometry and rapid mitosis ensure asymmetric episome segregation in yeast. *Curr. Biol.*, 21(1), 2011.
16. S. Levin-Zaidman, J. Englander, E. Shimoni, A. K. Sharma, K. W. Minton, and A. Minsky. Ringlike structure of the *Deinococcus radiodurans* genome: A key to radioresistance? *Science*, 299(254), 2003.
17. A. Lieber, A. Leis, A. Kushmaro, A. Minsky, and O. Medalia. Quasi-two-dimensional diffusion of single ellipsoids: Aspect ratio and confinement effects. *J. Bacteriol.*, 191, 2009.
18. O. Bénichou, M. Coppey, M. Moreau, P.H. Suet, and R. Voituriez. Averaged residence times of stochastic motions in bounded domains. *Europhys. Lett.*, 70(1), 2005.
19. S. Condamin, O. Bénichou, and M. Moreau. Random walks and Brownian motion: A method of computation for first-passage times and related quantities in confined geometries. *Phys. Rev. E*, 75, 2007.
20. Z. Schuss, A. Singer, and D. Holcman. The narrow escape problem for diffusion in cellular microdomains. *Proc. Natl. Acad. Sci. USA*, 104(41), 2007.
21. O. Kochubey, X. Lou, and R. Schneggenburger. Regulation of transmitter release by Ca^{2+} and synaptotagmin: insights from a large CNS synapse. *Trends in Neuroscience*, 34(5), 2011.
22. R. Schneggenburger, Y. Han, and O. Kochubey. Ca^{2+} channels and transmitter release at the active zone. *Cell Calcium*, 52(3-4), 2012.
23. C. Guerrier and D. Holcman. The dire strait time for hidden targets. *In prep.*, 2014.
24. K. Dao Duc, Z. Schuss, and D. Holcman. Oscillatory decay of the survival probability of activated diffusion across a limit cycle. *Phys Rev E Stat Nonlin Soft Matter Phys.*, 89(3), 2014.
25. Z. Schuss. *Theory and Applications of Stochastic Processes, an Analytical Approach*. Springer series on Applied Mathematical Sciences, 170, NY., 2010.
26. C. Nusslein-volhar. *Coming to Life - How Genes Drive Development*. Broché, 2008.
27. D. Holcman, N. Hoze, and Z. Schuss. Narrow escape through a funnel and effective diffusion on a crowded membrane. *Phys. Rev. E*, 84, 2011.
28. Y. Han, A. Alsayed, M. Nobili, and A.G. Yodh. Quasi-two-dimensional diffusion of single ellipsoids: Aspect ratio and confinement effects. *Phys. Rev. E*, 80, 2009.
29. F. Perrin. Mouvement brownien d'un ellipsoïde - I. Dispersion diélectrique pour des molécules ellipsoïdales. *J. Phys. Radium*, 5(10), 1934.
30. F. Perrin. Mouvement brownien d'un ellipsoïde (II). Rotation libre et dépolariation des fluorescences. Translation et diffusion de molécules ellipsoïdales. *J. Phys. Radium*, 7(1), 1936.
31. A.F. Cheviakov, M.J. Ward, and R. Straube. An asymptotic analysis of the mean first passage time for narrow escape problems: Part II: The sphere. *SIAM Multiscale Model. Simul.*, 8(3), 2010.